PCCP

Cite this: *Phys. Chem. Chem. Phys.*, 2011, **13**, 18485–18496

www.rsc.org/pccp

PAPER

Time-resolved predissociation of the vibrationless level of the B state of CH_3I

N. Thiré,[ab] R. Cireasa,[ab] D. Staedter,[ab] V. Blanchet*[ab] and S. T. Pratt[c]

Received 23rd June 2011, Accepted 31st August 2011
DOI: 10.1039/c1cp22057h

The predissociation dynamics of the vibrationless level of the first Rydberg 6s ($B\ ^1E$) state of CH_3I has been studied by femtosecond-resolved velocity map imaging of both the CH_3 and I photofragments. The kinetic energy distributions of the two fragments have been recorded as a function of the pump–probe delay, and as a function of excitation within the umbrella and stretching vibrational modes of the CH_3 fragment. These observations are made by using (2 + 1) Resonant Enhanced MultiPhoton Ionization (REMPI) *via* the $3p_z\ ^2A_2''$ state of CH_3 to detect specific vibrational levels of CH_3. The vibrational branching fractions of the CH_3 are recovered by using the individual vibrationally state-selected CH_3 distributions to fit the kinetic energy distribution obtained by using nonresonant multiphoton ionization of either the I or the CH_3 fragment. The angular distributions and rise times of the two fragments differ significantly. These observations can be rationalized through a consideration of the alignment of the CH_3 fragment and the effect of this alignment on its detection efficiency. Two additional dissociation channels are detected: one associated with Rydberg states near 9.2 eV that were observed previously in photoelectron studies, and one associated with photodissociation of the parent cation around 15 eV.

1. Introduction

Time-domain studies of the predissociation of Rydberg states of methyl iodide have primarily been performed by monitoring the decay of the parent ion signal produced by photoionization of the Rydberg states. Using this approach, the vibrationless level of the first optically active Rydberg state, namely the B 6s[2] state, was found to have a picosecond lifetime,[1,2] while higher vibrational levels of this state were found to have significantly shorter lifetimes.[3–5] Recently, we have studied the predissociation of the vibrationless level of the B 6s[2] state by time-resolved photoelectron spectroscopy,[6] and in the present paper, we extend this work by using fs-REMPI (Resonant Enhanced Multiphoton Ionization) to study the fragment branching fractions and translational energy distributions. The present results can be compared with the recent results of Gitzinger *et al.*, which were obtained by using a very similar experimental set-up.[7]

The B 6s[2] state is derived from the promotion of a 5pπ electron into a 6s Rydberg orbital, leaving a ground state $CH_3I^+\ ^2E_{3/2}$ ion core. Predissociation of the 6s Rydberg state may occur by spin–orbit interaction with the continuum of the anti-bonding σ* lowest unoccupied molecular orbital (LUMO) localized on the C–I bond. This σ* orbital is responsible for the well-known A band. Two dissociation channels are energetically allowed, leading to a ground state CH_3 radical and an iodine atom in either the $^2P_{3/2}$ ground state or the $^2P_{1/2}$ spin–orbit excited state. Hereafter, these two states are labeled I and I*, respectively. The corresponding dissociation thresholds have been determined to be 2.366 ± 0.013 eV and 3.309 ± 0.013 eV by a state of the art experiment that combined a hexapole to select the initial state and a velocity map imaging spectrometer to measure the distribution of the fragments.[8] The energetics of the neutral and ionic states of the CH_3I parent and its fragments are illustrated schematically in Fig. 1, along with the excitation schemes used to prepare the CH_3I and to detect its fragments. Vibrational excitation of the CH_3 is expected to populate the umbrella mode ($\nu_2 \approx 607\ cm^{-1}$) preferentially, owing to the transition from the nearly tetrahedral geometry of the CH_3 in CH_3I to the planar structure of the free CH_3 ground state. CH_3 fragments produced by photodissociation within the A band also show some activity in the ν_1 symmetric stretching mode ($\sim 3004\ cm^{-1}$),[9,10] and this may also occur following excitation to the B state.

Here we examine the predissociation of the vibrationless level of the B 6s[2] state by using time-resolved photoion velocity map imaging. The CH_3 and I fragments were selectively ionized by REMPI schemes that allow the determination

[a] *Université de Toulouse, UPS, 118 route de Narbonne, F-31062 Toulouse, France. E-mail: val@irsamc.ups-tlse.fr; Fax: +33 561 558 317*
[b] *CNRS, Laboratoire Collisions Agrégats Réactivité, IRSAMC, F-31062 Toulouse, France*
[c] *Argonne National Laboratory, Argonne, IL 60439, USA*

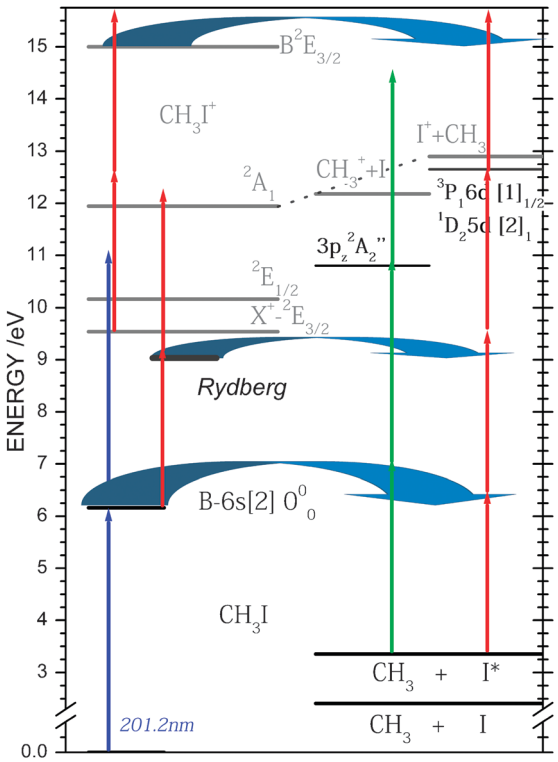

Fig. 1 Schematic diagram of the electronic states, dissociation limits, and photoionization thresholds encountered after excitation of the vibrationless level of the B state at 201.2 nm. The nascent CH_3 fragments are probed by (2 + 1) REMPI (green arrows) with typical wavelength around 330 nm and the iodine fragment is probed by four-photon ionization at 403 nm (red arrows).

of the vibrational distribution of the CH_3 fragment. The main new results presented here are the time-dependencies of the CH_3 fragments as a function of the polarisation of the probe, the angular distribution of CH_3, and two new channels of dissociation detected on the iodine distribution. These two channels correspond to dissociation *via* the Rydberg state at ~9 eV in a process that also produces a Rydberg fingerprint in the photoelectron spectrum, and to dissociation of the cation at an energy around 15 eV.

The remainder of the paper is organized as follows. A description of the experimental setup and the choice of probe wavelength are given in Section 2. Next, the CH_3 vibrational energy distribution is given in Section 3.1. The time dependences of the fragments as a function of their energies are summarized in Section 3.2. All the results are discussed in Section 4.

2. Experimental details

The experimental setup is a standard combination of a continuous molecular beam coupled to a Velocity Map Imaging (VMI) spectrometer and has been described previously.[6] The laser is a 1 kHz–3 mJ per pulse Ti:Sapphire regenerative-amplified system (Amplitude System), delivering pulses with a central wavelength of ~805 nm and a Fourier-transform-limited full width at half-maximum (FWHM) duration of ~70 fs. The 1.8 mJ per pulse dedicated to femtochemistry is divided into two parts. One part is used to generate the pump beam by using crystals to produce the fourth harmonic at 201.2 nm with a pulse energy of 1.5 μJ. This energy has been increased to 2.8 μJ for the investigation of the photodissociation of the cation. The second part is used to generate the probe beam by using a home-made Non-collinear Optical Parametric Oscillator (NOPA) with three stages of amplification. The NOPA delivers compressed pulses with 25 μJ of energy that are tunable between 510 and 700 nm. This output is then mixed with the 805 nm fundamental to generate tunable pulses between 313 and 340 nm with 7 μJ of energy, allowing the state-selective ionization of CH_3 with different numbers of quanta in the umbrella mode. The FWHM spectral bandwidths of 150 and 120 cm^{-1} for the pump and probe, respectively, result in a correlation time around ~160 fs, somewhat shorter than the experimental FWHM of ~300 ± 50 fs, depending on the probe wavelength. The pump and probe beams are focused onto the molecular beam by using 500 and 200 mm lenses, respectively. By measuring the spatial mode of the light pulses with a UV-CCD camera, the intensities of the two beams are found to be $<6 \times 10^{11}$ W cm^{-2}. Iodine detection is accomplished simply by photoionizing with the second harmonic of the fundamental pulse, *i.e.*, at 403 nm. The 403 nm light has a FWHM of 120 cm^{-1}, and a pulse energy of 35 μJ, corresponding to 3×10^{12} W cm^{-2}. This energy has been reduced to 5 μJ for the investigation of the photodissociation of the cation. In most of the experiments, the linear polarizations of the pump and probe are parallel to each other, and are also parallel to the face of the detector.

The continuous molecular beam is composed of a 10% CH_3I/Ar mixture, obtained by flowing 350 Torr of Ar through a CH_3I sample held at −30° Celsius. This mixture expands through a 250 μm nozzle, and the resulting molecular beam is collimated by two skimmers. Under these expansion conditions, there is no evidence for the formation of CH_3I clusters or I_2 in the mass spectrum or as additional features in the ion images, indicating that dimer formation is negligible.[5,11–13]

In the interaction region, the molecular beam is crossed at right angles by the laser beams. The charged species created in this region are extracted perpendicularly to the plane defined by the laser and the molecular beams, through a 40 cm time-of-flight tube and are projected onto the detector, which consists of two micro channel plates (MCP) of 40 mm coupled to a phosphor screen. Transient ion signals are recorded by integrating the signal collected from the phosphor, which was subsequently preamplified and sent to a gated boxcar integrator. At each pump–probe delay, the signal is averaged over 3×10^3 laser shots. The raw images, recorded by a 12 bit digital video camera, are reconstructed by using Abel transformations to provide the 3-D distributions. At selected pump–probe delays, higher quality images were recorded by averaging over 2×10^5 laser pulses. The CH_3 images have been recorded with 4 kV applied to the repeller, which typically results in a resolution of ~100 meV at a fragment translational energy of 2 eV. The iodine fragments were also recorded at a repeller voltage of 4 kV to allow a direct comparison to CH_3 distribution. In addition, to improve the energy resolution, images of iodine were also recorded at a repeller voltage of 2 kV (~20 meV at 0.5 eV).

The absorption spectrum of CH_3I is dominated by a single sharp peak at 6.16 eV (201.2 nm), and there is no evidence for

an absorption continuum within the laser bandwidth (150 cm^{-1}).[14] This situation ensures that only the $v = 0$ level of the B 6s[2] state is excited by one photon of the pump.

The I and CH_3 fragments were detected in different manners. Our optical set-up does not produce pulses of sufficient intensity at 304 nm to allow the state-selective ionization of I*, in contrast to the experiments of Gitzinger *et al.*[7] Instead, the iodine fragments are photoionized nonresonantly by using four photons at 403 nm. Several near resonances at three-photon energy could enhance this ionization process. These three-photon resonances include $^3P_1 6d[1]_{1/2} \leftarrow I^* \ ^2P_{1/2}$ at 74 425 cm^{-1}, $^1D_2 5d[2]_{1/2} \leftarrow I^* \ ^2P_{1/2}$ at 74 632 cm^{-1}, and $^3P_1 5d[1]_{3/2} \leftarrow I \ ^2P_{3/2}$ at 74 587 cm^{-1}.

The CH_3 fragment is produced in the $2p_z\ ^2A_2''$ electronic ground state and is probed either by nonresonant ionization at 800 nm, nonresonant four-photon ionization at 403 nm, or resonant (2 + 1) ionization *via* the $3p_z\ ^2A_2''$ Rydberg state. For the resonance ionization experiments, the wavelength was tuned into resonance with the Q branch band heads, corresponding to absorption of two-photons at 333.45 nm for the 0_0^0 band, at 329.5 nm for the 2_1^1 band (ν_2 is the umbrella mode), at 326.1 nm for the 2_2^2 band, and at 322.8 nm for the 2_3^3 band.[15,16] The effective FWHM bandwidth for the two-photon absorption is 170 cm^{-1}, which is significantly smaller than the offset between successive sequence bands, thus allowing vibrational state selective ionization. This probe bandwidth is also sufficiently broad to overlap the entire Q branch within each umbrella band, and its duration is short enough to compete efficiently with the predissociation of the intermediate $3p_z\ ^2A_2''$ Rydberg state into CH_2 + H. Note, however, that the bandwidth of the probe at the wavelength for the 0_0^0 band does overlap the 1_1^1 symmetric stretch band and the 3_1^1 degenerate asymmetric stretch band, both of which occur at 2 × 333.9 nm.[17]

3. Results

The time-transient of CH_3I is characterized by a single exponential decay with a time constant $T_e = 1.31 \pm 0.07$.[6] The time-resolved transients of the fragments already shown in ref. 6 are fitted by considering two contributions, one for the dissociative ionization process, and a second rising component for the predissociation as given by:

$$S_{frag^+}(t) = a_0 + (1 + \mathrm{erf}(\phi(t, T_e))) \times b_0 e^{-\frac{t-t_0}{T_e}} + (1 + \mathrm{erf}(\phi(t, T_r))) \times c_0 \left(1 - e^{-\frac{t-t_0}{T_r}}\right) \quad (1)$$

with the error function, $\phi(\Delta t, T)$, defined as:

$$\phi(t, T) = \frac{2\sqrt{\ln 2}}{T_{cc}} \left(t - \frac{T_{cc}^2}{8 \ln 2 \times T}\right). \quad (2)$$

Here T_e is the decay time of the parent and T_r is the rise time of the fragment. The cross-correlation time T_{cc} fixed to the measured value of 300 ± 50 fs and the t_0 a shift of appearance relative to the "zero delay" are determined by a non-resonant pump–probe ionization of NO.

3.1 Energy distribution of photofragments at 8 ps delay

Fig. 2 shows velocity-map ion images for I and CH_3 recorded with a pump–probe delay of 8 ps. The single-color background has been subtracted from these images. Fig. 2a shows reconstructed slices of the three-dimensional velocity distribution of iodine obtained by using the Abel transformation. With an energy of excitation at 6.16 eV,[18] the maximum available energy is 3.80 eV for the I channel, and 2.86 eV for the I* channel. The transition from the ground state to the B 6s[2] state has a perpendicular character. Thus, for predissociation that is slightly faster than the rotational period of the parent, the fragments issued from a non-vibrating parent are expected to be preferentially ejected perpendicular to the polarization axis of the pump beam, as can be seen for the image recorded for I fragments shown in Fig. 2a.

In contrast, independent of the probe wavelength, the CH_3 images exhibit different angular distributions (Fig. 2b and c). These distributions are far more anisotropic than the iodine image, with minimum intensities at the poles and equators that

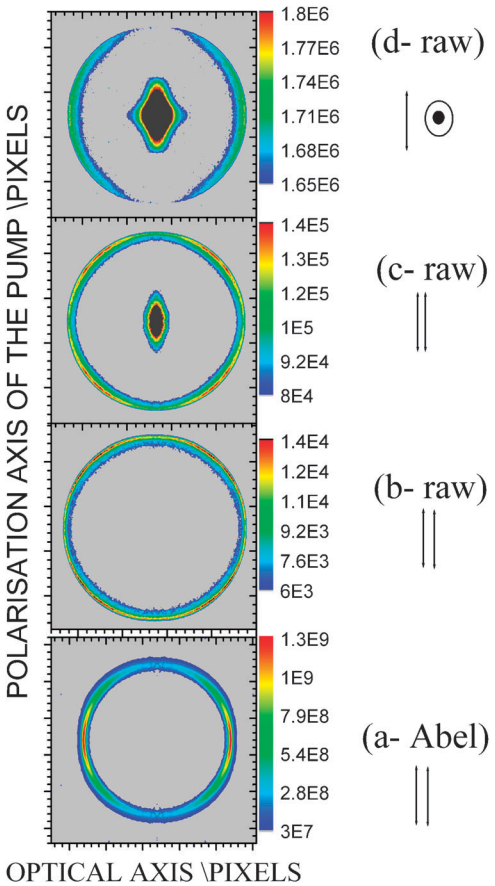

Fig. 2 (a) Abel inverted image of iodine fragments recorded at 8 ps delay with a 403 nm probe with polarization parallel to that of the pump. (b–d) Raw images of the CH_3 fragment recorded at 8 ps delay with a probe centered at (b) 333.5 nm and (c) 403 nm, both with the probe polarization parallel to that of the pump. (d) Raw CH_3 image recorded with a 403 nm probe with polarization perpendicular to that of the pump. All images have been symmetrized and the backgrounds have been subtracted. The repeller voltage was fixed at 2 kV for I images and at 4 kV for CH_3 images.

give the CH_3 images a four-fold symmetry. This observation is at first surprising because the conservation of momentum in the dissociation process requires the angular distribution of the CH_3 fragments to mirror that of the I fragment. Indeed the predissociation at 201.2 nm leads to the I* fragment with $J = \frac{1}{2}$ as we will discuss further, and this fragment cannot be aligned. As a result, the I* detection efficiency should be independent of the angle between the fragment velocity vector and the polarization axis, and the observed I^+ angular distribution should reflect the true angular distribution. The different observed angular distribution for the CH_3^+ image thus indicates the presence of an angular dependence of the detection efficiency of the CH_3. Importantly, the similarity of the angular distributions at 333.5 nm (as well as 329 nm not shown here) and 403 nm suggests that the transition moments for both processes have similar symmetry characteristics in common. In particular, the resonant two-photon process at 333.5 nm is known to be parallel transition, suggesting that the nonresonant ionization at 403 nm also is dominated by a parallel process. In fact, the three-photon energy at 403 nm is closest to resonance with the known $A_1'(5d)$ state of CH_3 at 75 000 cm^{-1}, which would serve to enhance the parallel character of this detection scheme. The lack of intensity at the poles of the CH_3 distribution suggests a lower detection probability for the fragments flying perpendicularly to the probe laser polarisation axis due to an unfavourable alignment of the CH_3 transition dipole moment and rotational angular momentum relative to the probe polarization. This alignment can be confirmed by recording an image with the probe polarization perpendicular to the pump polarization. An image recorded in this configuration at 403 nm is shown in Fig. 2d, with a strong CH_3^+ signal observed perpendicular to the pump polarization as expected. Alignment of the CH_3 fragment rotational angular momentum has been observed previously for photodissociation of CH_3I within the A band,[19,20] and similar angular distributions were also attributed to alignment effects in the two-photon dissociation of Rydberg states in CH_3Br.[21] To our knowledge, the observations reported here represent the first detection of angular momentum alignment using broad band fs lasers and imaging techniques. These effects will be discussed in more detail in a forthcoming paper.

Fig. 3 shows the total translational energy distributions extracted from the images for nonresonant ionization of I and CH_3 (Fig. 3a and b, respectively), and for resonant ionization of CH_3 ν_2 = 0, 1, and 2 (Fig. 3e, d, and c, respectively), at a pump–probe delay of 8 ps. Both our previous work[6] and the work of others[7] indicate that the dominant dissociation channel for the B 6s[2] state is to CH_3 + I*. The images for state-selective ionization of CH_3 allow us to assign the dominant peak in the corresponding translational energy distributions and thus internally calibrate Fig. 3c–e in a straightforward fashion. An accurate value for that dissociation threshold (D_0 = 3.309 ± 0.013 eV) has been determined from studies of the A band.[8] With this assignment, the calibration of the nonresonant CH_3 and I translational energy distributions follows directly. While the absolute accuracy of the internal calibration is not expected to be as good as that obtained by using an external standard, for the present study the most important aspect is the relative calibration. This relative calibration is expected to be quite good, as all of the images were recorded under the same

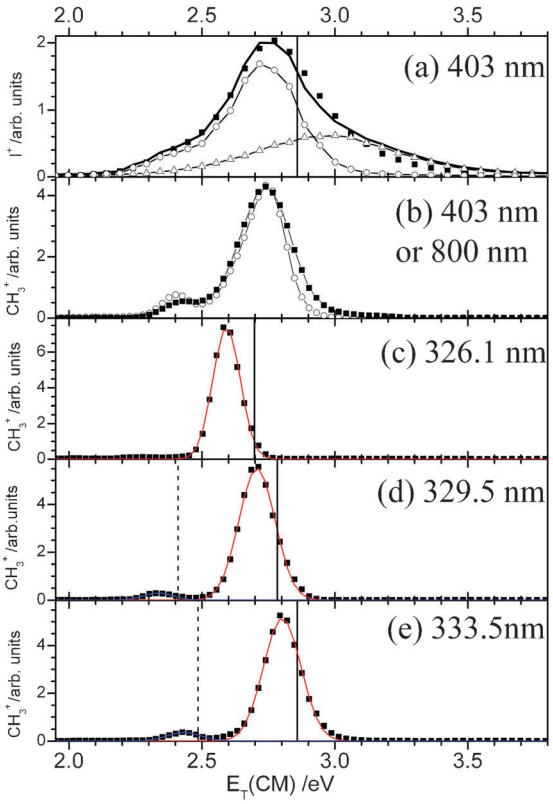

Fig. 3 Normalized energy distributions plotted as a function of the translational energy of the center of mass and recorded for different probe wavelengths at 8 ps pump–probe delay. (a) Full square: Iodine fully integrated over 360° of the Abel inverted image. Circle: Iodine integrated over a 20° range about the perpendicular to the pump polarisation with a weight of 0.61. Triangle: Iodine integrated over a 20° range about the direction parallel to the pump polarisation with a weight of 0.3. The 0.61 and 0.3 weights have been obtained by fitting the total distribution (over 360°). The full line corresponds to the sum of the perpendicular and parallel contributions, and should be compared to the full integration over 360°. The vertical line at 2.86 eV corresponds to the threshold limit at one photon for CH_3 + I*. (b) CH_3 ionized by four photons at 403 nm off resonance (empty circle) or seven photons at 800 nm (filled square). (c–e) CH_3 detected by (2+1) ionization (c) at 326.1 nm *via* the 2_2^2 resonance of the $3p_z\,^2A_2''$ state, (d) at 329.5 nm *via* the 2_1^1 resonance of the $3p_z\,^2A_2''$ state, (e) at 333.5 nm *via* the 0_0^0 resonance of the $3p_z\,^2A_2''$ state. The Gaussian fits in red and blue are used in the fit of the vibrational distributions shown in Fig. 5. The full vertical lines correspond to the translational energy expected for ($n \times \nu_2$) while the dashed ones correspond to ($n \times \nu_2 + \nu_1$) progressions, respectively.

conditions. With this calibration, it is also clear from Fig. 3 that there is no obvious contribution from dissociation to the lower energy CH_3 + $I(^2P_{3/2})$ products. This observation is consistent with our earlier results obtained from photoelectron spectra.[6]

The comparison of the translational energy distributions from the nonresonant I and CH_3 images is revealing. In particular, the I distribution in Fig. 3a extends to significantly higher energy than the CH_3 distribution in Fig. 3b, exceeding the thermodynamical threshold. This aspect of the distribution was not reported in ref. 7, but the pulse energies in the present experiment are somewhat higher than those the earlier experiment, which would increase the likelihood of multiphoton processes leading to our observation. Nevertheless, plotting

the I distribution of Gitzinger *et al.*[7] against the total translational energy (rather than the fragment translational energy) does suggest a behavior similar to that observed here. Also, their I image (10 ps delay) closely resembles the image presented in Fig. 2a (8 ps delay), featuring a strong contribution perpendicular to the pump laser polarisation overlapping a weaker isotropic or parallel contribution, and thus, a similar angular distribution should be expected. Because of the difference in pulse energies and focusing conditions, and because the details of the angular distribution for this tail are hard to extract from ref. 7, we focus further only on the present data. The present CH_3 distributions recorded with probe wavelengths of 400 nm and 800 nm are similar, indicating that these two detection schemes are essentially nonresonant. Interestingly, the translational energy distributions of iodine are different if the angular integration of the Abel image is limited to angles close to directions parallel or perpendicular to the pump polarisation (see Fig. 3a). Because the I* fragment cannot be aligned, this difference indicates that two processes with different angular distributions are contributing to the I image and its translational energy distribution. Fig. 4 shows the angular distributions obtained from I^+ images recorded with a pump–probe delay of 8 ps and corresponding to different translational energies (Fig. 3a). The corresponding anisotropy parameters are $\beta = -0.549 \pm 0.005$ for total translational energy of the iodine fragment between 2.2 eV and 3.0 eV, and $\beta = +0.89 \pm 0.02$ for fragment energies between 3 eV and 3.8 eV. While the process

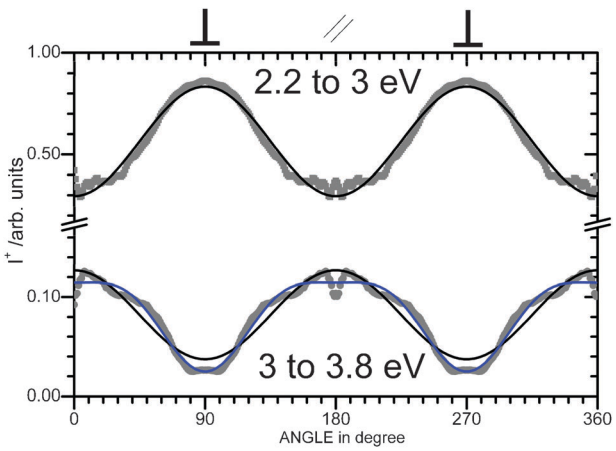

Fig. 4 Angular distribution of iodine at 8 ps pump–probe delay and recorded at the translational energy corresponding to the maximum of signal between 2.2–3 eV (square, $\beta = -0.549 \pm 0.005$), and at higher energy between 3 to 3.8 eV (circle, black line with $\beta = +0.89 \pm 0.02$ or blue line $\beta_2 = +1.02 \pm 0.01$ and $\beta_4 = -0.33 \pm 0.01$). The angle 180° corresponds to iodine emitted along the pump polarization.

corresponding to lower translational energies clearly corresponds to the ionization of I* fragment produced by predissociation of the B 6s[2], the nature of the process producing higher translational energies is discussed in Section 4.2.

Fig. 3c–e shows the energy distributions recorded using probe wavelengths of 326.1, 329.5 and 333.5 nm corresponding to the 2_2^2, 2_1^1 and 0_0^0 bands, respectively, of the (2 + 1) REMPI transition involving the $3p_z\,^2A_2''$ Rydberg state as a resonant step.[15,22] Attempts to record an image with the probe wavelength tuned into resonance with the 2_3^3 band at 322.8 nm were unsuccessful, suggesting that the predissociation process does not generate detectable amounts of $CH_3(\nu_2 = 3)$. This is confirmed by the CH_3 distribution recorded with a nonresonant probe. The typical widths of the translational energy distributions in Fig. 3c–e vary between 165 and 85 meV. The vertical full lines in Fig. 3 indicate the energy threshold expected for the fragment vibrational energy corresponding to bending excitation (ν_2 progressions). The ν_1 contribution is probed by (2 + 1) REMPI *via* the 1_1^1 band using 333.9 nm wavelength, which lies within the bandwidth of the 333.5 nm light used for the 0_0^0 band. As already observed at 193.3 nm, in the predissociation of the $\nu_2 = 2$ level of the 6s[2] state,[23] the CH_3 distribution is characterized by significant excitation of the symmetric stretching mode ν_1. In Fig. 3, the dashed lines indicate the threshold for excitation to the $\nu_1 + \nu_2$ combination mode, which was observed and assigned in previous fs studies of A and B band dissociations by Nalda *et al.*[10] and Gitzinger *et al.*[7] Nevertheless, REMPI transitions involving the $\nu_1 + \nu_2$ bands are not spectroscopically known.

The vibrationally state-selected translational energy distributions of Fig. 3c–e have been used to fit the translational energy distributions from both the I and CH_3 images (Fig. 3a–b) recorded nonresonantly, and thus provide a determination of the CH_3 vibrational distribution. This distribution is summarized in Table 1 and Fig. 5. The vibrational distribution found for CH_3 recorded off resonance at 403 nm or 800 nm is the same. In contrast to Gitzinger *et al.*[7] who directly used in their fits the translational energy distributions measured resonantly, as only one component, we have used normalised functions resulting from the fit of each vibrational component observed in Fig. 3. This approach completely decouples the contributions of each vibration and thus eliminates the possible artifacts in the relative intensities produced by variations in the detection efficiencies of the ν_1 and ν_2 components. The $\nu_2 = 1$ feature is the largest component of both vibrational distributions presented in Fig. 5, but there is also significant intensity in the $\nu_2 = 0$ component. In contrast, in the vibrational distribution reported by Gitzinger *et al.*, the $\nu_2 = 0$ component is dominant. This difference might just result from the fitting procedure.

Table 1 Vibrational distribution at 8 ps resulting from the fit performed on the iodine and CH_3 translational energy distributions recorded with a probe centered at 403 nm or 800 nm. The translational energy distribution of the iodine fragments that is fitted is the one obtained by integrating over the angles within 20° of the perpendicular to the pump polarization

%	$(\nu_1, \nu_2) = (0, 0)$	$(\nu_1, \nu_2) = (0, 1)$	$(\nu_1, \nu_2) = (0, 2)$	$(\nu_1, \nu_2) = (1, 0)$	$(\nu_1, \nu_2) = (1, 1)$
I_{perp}	30 ± 3	30 ± 3	15 ± 2	10 ± 2	4 ± 2
CH_3 at 403 nm	36 ± 1	44 ± 1	9 ± 1	7 ± 1	—
CH_3 at 800 nm	28 ± 2	56 ± 2	4 ± 2	10 ± 2	2 ± 1
Ref. 7	37	28	24	7	4

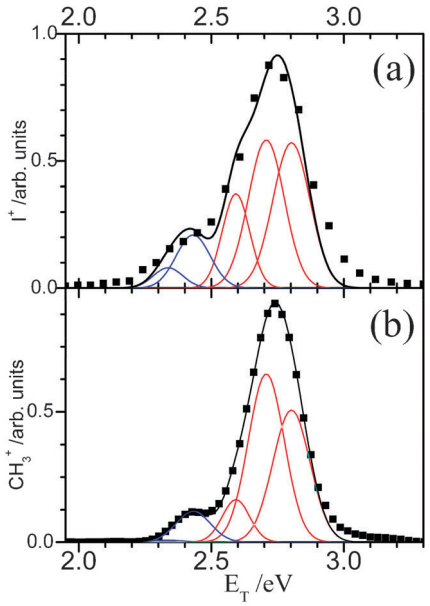

Fig. 5 Fits of the vibrational distribution recorded at 8 ps delay using (a) iodine integrated over 20° perpendicular to the pump polarization (Fig. 3a) and (b) CH_3 recorded off-resonance at 403 nm (Fig. 3b). The vibrational distributions are summarized in Table 1.

3.2 Rise time of the neutral fragments

Fig. 6 shows the time dependence of the fragment signals as a function of the pump–probe delay. The curves for I and CH_3 have been recorded in two and three independent scans, respectively. These time-dependences are fitted by the rising function of eqn (1) (*i.e.*, the term that includes c_0), except for that from Fig. 6b. The latter decay process is fitted by a cross-correlation function and a decaying exponential that multiplies the term in b_0 of eqn (1). The time constants and time shifts extracted by fitting the data are summarized in Table 2.

Iodine fragment. The iodine translational energy distribution is characterized by three different contributions: one corresponding to fragments emitted perpendicular to the pump polarisation at 2.8 eV and two corresponding to fragments emitted parallel to the pump polarisation at 3 eV and 6.4 eV. These three components have different time-dependences, as shown in Fig. 6a–c respectively.

Perpendicular component around 2.8 eV—Fig. 7a. The iodine fragments emitted between 80°–100° (perpendicular to the pump polarisation) appear within 1.17 ± 0.06 ps and have a translational energy of about 2.8 eV (Fig. 6a). As expected by taking into account the shift of appearance, these fragments have an overall appearance time corresponding to the decay time of the parent ion.

Parallel component around 3 eV—Fig. 7c. The time dependence of the iodine fragments emitted parallel to the pump polarisation within a 20° angle and with a energy around 3 eV (see Fig. 6c) can be split in two parts: a step function with a rising edge corresponding to the laser cross-correlation and an increasing

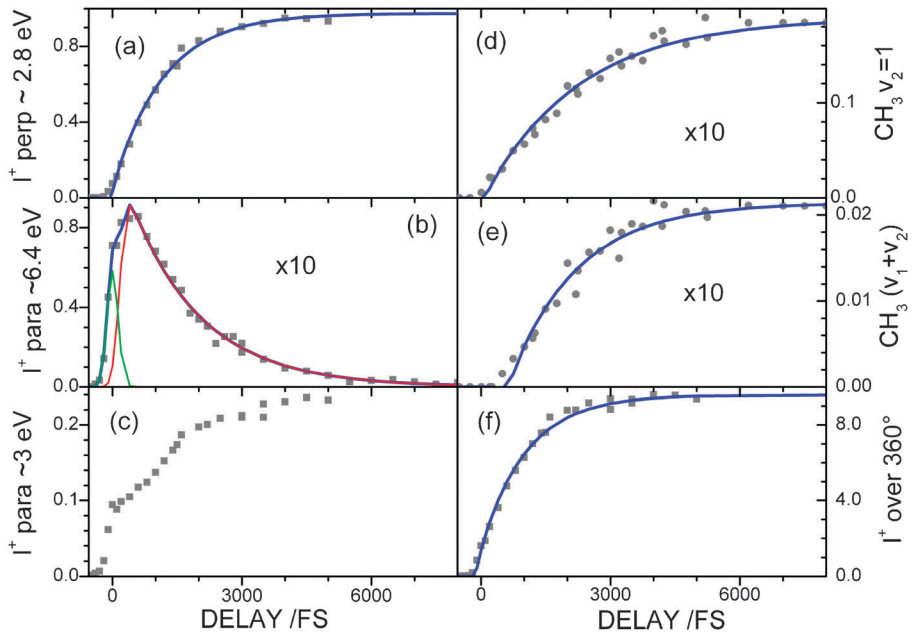

Fig. 6 Time dependences of the fragments emitted with different kinetic energies and ejection angles. (a) Iodine fragments integrated over a 20° angle about the perpendicular to the pump polarization and for translational energies between 2.3 and 3.3 eV. These data have been recorded in two scans. (b–c) Iodine fragments integrated over a 20° about the direction parallel to the pump polarization and for translational energies within a 2 eV window centered (b) at 6.4 eV and (c) at 3 eV. (d) CH_3 fragments recorded with a probe centered at 329.5 nm. The *y*-scale corresponds to the intensity of the component $\nu_2 = 1$ recorded *via* the REMPI 2^1_1 and extracted from a fit of the energy distribution performed for each delay. These data have been recorded in three scans. (e) CH_3 fragments recorded with a probe centered at 329.5 nm. The *y*-scale corresponds to the intensity of the component assigned to $\nu_2 + \nu_1$ combination mode and extracted from a fit of the energy distribution done for each delay. (f) Iodine fragments integrated over 360° and within a 2 eV window centered at 3 eV. The relative intensities of the transients have been maintained through the normalization of the *y*-scale. This is specifically relevant to compare a–c or f, as well as independently d and e.

Table 2 Time dependences extracted from the fits of the energy resolved signals of Fig. 6 or of Fig. 9. The fits have been performed with a cross-correlation time around 300 ± 50 fs. I_{perp} and I_{para} correspond to the intensity of iodine collected perpendicularly and parallel to the pump polarization within a 20° angle. In Fig. 6, the pump and probe polarizations are parallel, while in Fig. 9, they can be parallel or perpendicular

	Time constant T_r/ps	Shift of the appearance t_0/fs
Fig. 6—Pump–probe para.		
(a) $I_{perp} \approx 2.8$ eV	1.17 ± 0.06	193 ± 20
(b) $I_{para} \approx 6.4$ eV	Decay: 1.65 ± 0.05	164 ± 10
(f) I over 360°	1.05 ± 0.05	83 ± 19
(d) CH_3 $v_2 = 1$	2.24 ± 0.12	307 ± 52
(e) CH_3 $v_2 + v_1$?	1.57 ± 0.11	910 ± 60
Fig. 9		
CH_3 @ 403 nm pump–probe para.	2.02 ± 0.15	157 ± 65
CH_3 @ 403 nm pump–probe perp.	1.36 ± 0.07	249 ± 36

function with a rise time on the picosecond scale. Note that the perpendicular contribution with $\beta = -0.549$ will lead to a contribution in the 20° parallel distribution of about 36% of what is emitted perpendicular but centered on 2.75 eV. Fig. 3a recorded at 8 ps shows a percentage roughly 27% at 2.75 eV to compare to the expected 36%, while at 3 eV, around 2.5 times more iodine atoms are produced parallel instead of perpendicular. This observation leads us to conclude that another process takes place on a picosecond time scale in addition to the predissociation from the $v = 0$ of the B 6s[2] state, and that this second process is not observed in the CH_3 product channel. To enhance this contribution, images were recorded with the pump energy increased to 2.8 μJ and the probe decreased to 5 μJ. Fig. 7 shows two corresponding Abel inverted images recorded at 1 ps and 8 ps as well as the energy distribution obtained by integration over a 20° angle around the pump polarisation and the energy distribution emitted perpendicularly to the pump polarisation at 8 ps.

Parallel component around 6.4 eV—Fig. 6b and 8. The energy distribution of iodine fragments emitted along the pump polarisation at high energy is shown in Fig. 8. The time-dependence of

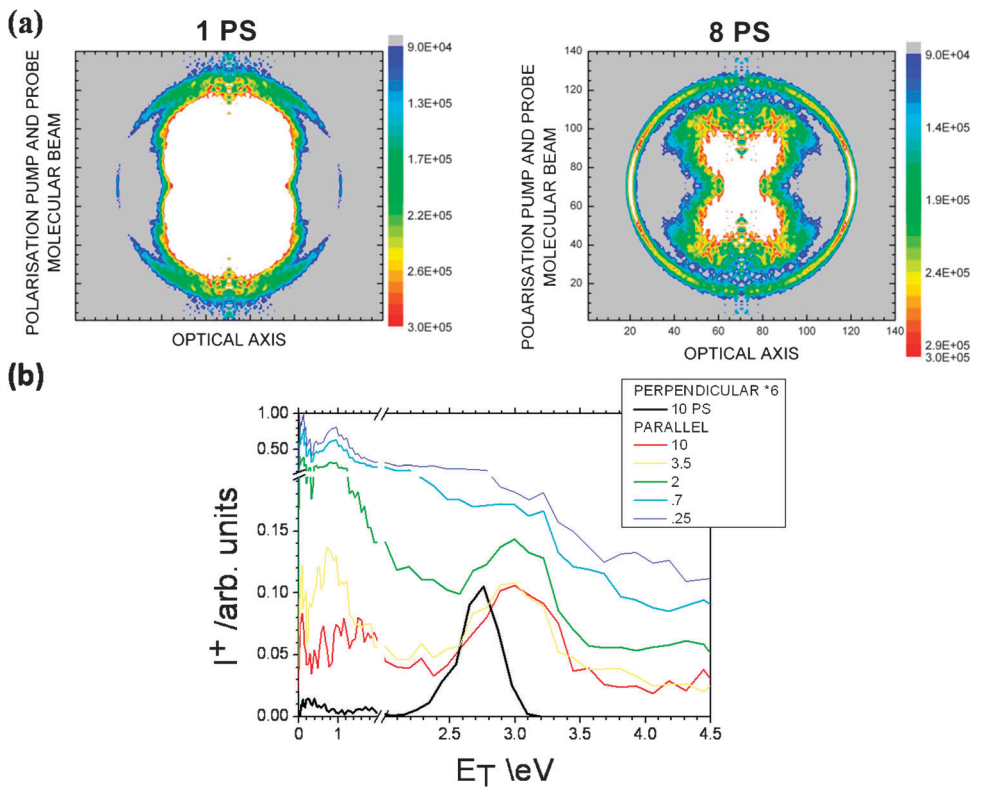

Fig. 7 Iodine fragments recorded with a higher pump energy at 2.8 μJ and a lower probe energy at 5 μJ to enhance the dissociation dynamics taking place in the ion continuum. The pump and probe polarizations are parallel to each other and perpendicular to the time-of-flight axis. (a) Abel images recorded a 3 kV for the repeller voltage for two different delays. Clearly, at 1 ps the outer ring is aligned along the pump and probe polarization while at longer delay a new component appears with roughly the same energy but pointing perpendicular to the pump polarization. This new component corresponds to the fragments that have been photoionized after the predissociation from the B 6s[2] Rydberg state and masks the parallel contribution. (b) The translational energy distribution recorded for iodine fragments ejected within a 20° angle of the pump polarization as a function of the pump–probe delay and compared to the one recorded at 10 ps within a 20° angle perpendicular to the pump polarization (black plot).

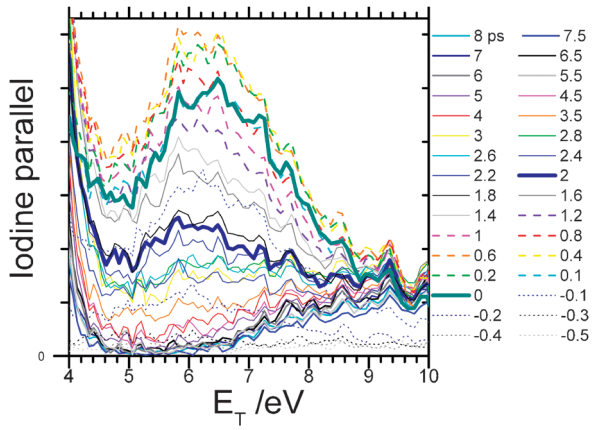

Fig. 8 Translational energy of the iodine fragment obtained by integration of the Abel inverted image over a 20° angle around the pump polarization and for different pump–probe delays. The integrated intensity corresponding to the component centred at 6.4 eV has the time-dependence shown in Fig. 6b.

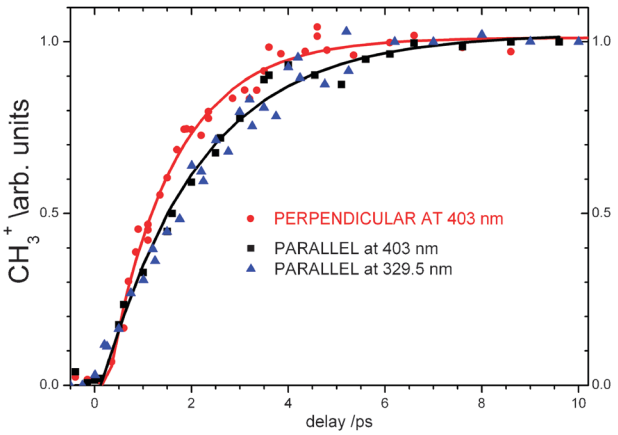

Fig. 9 Time dependences of the CH_3 fragments ejected with kinetic energy between 2.3 and 3.2 eV (see Fig. 3b) recorded for two configurations for the polarization of the pump and probe pulses, where the probe polarization is either parallel or perpendicular to the pump polarization and detector plane. The black squares and blue triangles represent measurements taken in a parallel configuration using probe wavelengths of 403 nm and 329.5 nm, respectively. The red circles correspond to data taken with a 403 nm probe in a perpendicular configuration. The parameters deduced from the fits are listed in Table 2.

this iodine shown in Fig. 6b can be fitted by a cross-correlation function with an exponential decay on the time scale 1.65 ± 0.05 ps slightly longer than the CH_3I^+ decay 1.31 ps. We assigned this component to the iodine fragment produced around 9.24 eV by the absorption of one probe photon from the $v = 0$ level of the B 6s[2] state. This (1 + 1′) excitation path was already identified in the photoelectron spectrum *via* a Rydberg fingerprint onto the 6p[2,4] and 7s[2,4] states.[6] The vibrational energies in these Rydberg states are 1.92 eV in 6p[2] and 1.21 eV in 7s[2], and these states are expected to have very short lifetimes. Indeed the lifetimes of their vibrationless levels have been measured to be shorter than 150 fs.[24] These two ultrafast radiationless transitions would produce fragments with total available energies of 5.93 eV for the I* channel and 6.88 eV for the I channel, respectively. The production of iodine in its ground state can come from the interaction with the repulsive $^1Q(E)$ as predicted by the calculations for energy larger than 6.8 eV.[25] The anisotropy parameter obtained by fitting the angular dependence of the iodine translational distribution between 4.5 and 7 eV at a delay of 700 fs is β = 1.89 ± 0.05. The kinetic energy of the CH_3 fragments associated with this process is so high that the corresponding ring in the image is larger than the diameter of the detector, and is thus not observed. To a first approximation, the lifetime of this component should reflect the lifetime of the $v = 0$ of the B 6s[2] state, since this state is an intermediate in accessing the 9.4 eV resonances. It is noteworthy that this process occurs within the probe pulse duration and requires five photons of the probe with two resonant steps.

Methyl fragment. The time dependence of the CH_3 full vibrational distribution was recorded using nonresonant ionization at 403 nm (see Fig. 9). In addition, the methyl produced in the (ν_1, ν_2) = (0,1) vibrational state and detected with a probe pulse centered at 329.5 nm has been recorded as a function of the pump–probe delay. The translational energy distribution recorded at 329.5 nm does not change in time and results in the distribution shown in Fig. 3d, which was fitted by two Gaussian distributions: one peaking at 2.7 eV and corresponding to one quantum excitation of the umbrella mode (ν_1, ν_2) = (0, 1) (REMPI (2 + 1) transition at 329.5 nm) and the second one around 2.35 eV that we assign as Gitzinger *et al.*[7] to an excitation of the combination mode (ν_1, ν_2) = (1, 1). As noted above, this observation would indicate that within the broad bandwidth of the probe pulse, a REMPI (2 + 1) transition probing this combination mode is expected in this wavelength region, however this has never been identified spectroscopically. Surprisingly both of these components have rise times that are considerably longer than any other timescales measured (T_r = 2.2 ps, see Table 2), especially when taking into account the shift of appearance time. The increase in the rise time is not an experimental artefact, as the same time dependence was obtained for three different experimental runs. As illustrated in Fig. 9, the same behavior (T_r = 2 ps) was also observed for the time dependence of the fragments ionized at 403 nm which probes all the vibrational states of methyl.

4. Discussion

In general, our data are in good agreement with the recently published results of Gitzinger *et al*. The observation that only I* fragments are detected from the predissociation of $v = 0$ of the B 6s[2] state confirms the conclusions of the previous works.[7,23,26,27] This conclusion can be understood easily for the B 6s[2] vibrationless level by considering the crossing of the potential surfaces of the B 6s[2] state and the $4E(^3A_1)$ and $^2A_2$ ($^3A_1$) valence states along the C–I stretching coordinate. Both the 4E and $^2A_2$ valence potential surfaces cross the B 6s[2] surface near its equilibrium geometry, and both diabatically correlate with the CH_3 + I* dissociation limit.[25,28] The β_2 of I* produced at 2.8 eV is −0.549 ± 0.005 (Fig. 4) similar to the −0.5 reported by Gitzinger *et al*. The predissociation is

caused by the spin–orbit coupling. The present vibrational state distribution differs slightly from the one of Gitzinger *et al*., but can be understood in terms of the different fitting procedures used for the CH_3 translational energy distributions.

4.1 The time dependence of CH_3 fragments

We have measured for the first time, the temporal dependence of CH_3 fragments produced in the dissociation of the $v = 0$ level of the B 6s[2] state. The rise time for the signal corresponding to CH_3 (ν_1, ν_2) = (0, 1) umbrella mode and parallel polarization of the probe beam is 2.24 ± 0.12 ps, which is considerably longer than expected based on that of the corresponding I* signal or either the decay time of the parent ion. A similar rise time of 2.02 ± 0.15 ps is observed for the signal corresponding to ionization at 403 nm with parallel polarization (Fig. 9). In order to rationalize this observation we propose a model which accounts for the CH_3 detection sensitivity as a function of the relative alignments of transition dipoles used to photodissociate the CH_3I and to photoionize the CH_3 fragment with respect to the polarizations of the pump and the probe. In the following discussion, it is assumed that the C_{3v} symmetry group is preserved during the predissociation of CH_3I. The transition dipole moment of the B 6s[2] $\leftarrow {}^1A_1'$ transition at 201.2 nm is perpendicular to the C_3 axis of the CH_3I and thus preferentially selects molecules with the C_3 axis lying in the plane perpendicular to the pump polarisation and parallel to the time-of-flight. Thus, if the dissociation is prompt, the C_3 axis of CH_3 fragment is (at least initially) parallel to the C_3 axis of CH_3I, and perpendicular to the polarization axis of the probe light, which is parallel to the polarization of the pump in this configuration. However, the transition dipole moment of the two-photon $3p_z{}^2A_2'' \leftarrow 2p_z{}^2A_2''$ step in the (2 + 1) REMPI used to detect the CH_3 is parallel to the C_3 axis of the CH_3. Similarly, as discussed in Section 3.1, the transition dipole of the 403 nm ionization scheme appears to be dominated by parallel character, most likely *via* near resonance with the three-photon ${}^2A_1'(5d) \leftarrow {}^2A_2''$ transition. Consequently, for a prompt dissociation, the initial ionization probability is expected to be almost zero because the probe polarisation is perpendicular to the dipole moment of detection transition. However, the present dissociation is not a prompt process, but rather a predissociation taking place over 1.3 ps. This process is thought to involve a slow crossing onto the σ* surface, followed by rapid (<100 fs) dissociation on that surface. Therefore, one factor that can diminish this C_3 axis alignment effect is the rotation of the parent molecule before the dissociation takes place. Following this, the C_3 axis of the CH_3I will be no longer perpendicular to the probe polarisation, and the CH_3 fragments will be ejected over a greater range of angles relative to the probe polarization. Our main hypothesis is that the resulting position of the C_3 axis relative to the polarization of the probe laser has the potential to modify the appearance of this fragment. We will now discuss this in more detail.

Although the sample is cooled in a molecular beam, the rotational temperature cannot be ignored. We will label T_{rot}^* the temperature corresponding to the angular energy causing CH_3I to leave the plane selected by the pump transition and this corresponds to rotation about a C_2 axis. This rotation is the one that contributes most to the loss of anisotropy in the detection process. This T_{rot}^* can be deduced from the angular distribution of the I* fragment. If it is assumed that the B 6s[2] $\leftarrow {}^1A_1'$ transition is purely perpendicular, we assume that the deviation of the value of β from the limiting value of −1 to −0.549 ± 0.005 (Fig. 4) is due to rotation of the parent molecule outside of this plane selected by the pump transition. By treating classically the parent rotation, the angular distribution of the iodine fragment for a one-photon perpendicular transition can be written:[29,30]

$$\Gamma(\theta) = \frac{1}{4\pi}(1 + \beta(T_e)P_2(\cos\theta))$$
$$\text{with } \beta(T_e) = \beta(0)\frac{1 + (\omega T_e)^2}{1 + 4(\omega T_e)^2} \quad \text{and} \quad \beta(0) = -1 \tag{3}$$

For which the rotational energy is:

$$E_{rot} = \frac{I_b\omega^2}{2}$$

with the main moment of inertia for the C–I rotation I_b = 111.8 × 10^{-47} kg m^2 and the predissociation time T_e fixed to 1.3 ps in agreement with the decay time of the parent. Once integrated over the possible rotational energies taking into account their Boltzmann distributions, we get

$$\Gamma(\theta) \propto \frac{\sqrt{\pi}(3 - \cos^2(\theta))}{16T_e\mu} + \frac{\pi[1 - \phi(\mu/2)]\exp(\mu^2/4)}{8T_e} \times \left(\sin^2(\theta) - \frac{(3 - \cos^2(\theta))}{4}\right) \tag{4}$$

with

$$\mu^2 = \frac{I_b}{2T_e^2 k_B T_{rot}^*},$$

and where $\phi(x)$ is the error function. This angular dependence can then be fitted by

$$\left[1 + \frac{\beta}{2}(3\cos^2(\theta) - 1)\right],$$

as done for the experimental results. Fig. 10 gives the anisotropy parameter β for the predissociation time of 1.3 ps. The anisotropy parameter β = −0.549 results from T_{rot}^* = 62 K, to which we can associate an averaged rotational period around the C_2 axis, given by:

$$\left(\frac{2\pi\sqrt{\pi I_b}}{\sqrt{2k_b T_{rot}^*}}\right),$$

of 9 ps. Note that the extracted rotational period is not particularly sensitive to the predissociation time, and the rotational period changes by only ~1 ps for an increase in predissociation time of 100 fs.

Assuming that the predissociation time is 1.3 ps, the C_3 axis will start to be aligned with the probe polarization after a quarter of a rotational period, *i.e.*, ~2.25 ps. The observed rise time of the $CH_3(\nu_2 = 1)$ of 2.24 ps is consistent with this process. As far as we know the only angular dependence reported for the methyl fragments resulting from the Rydberg

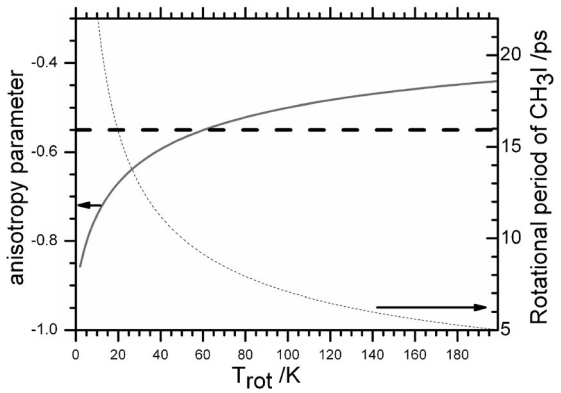

Fig. 10 The left axis shows the anisotropy parameter β as a function of T^*_{rot} of CH_3I for a predissociation time of 1.3 ps. The horizontal line at $\beta = -0.549$ corresponds to the anisotropy measured in Fig. 4 for iodine emitted with E_T = 2.2–3 eV. The right axis shows the rotational period of CH_3I as a function of T^*_{rot}. For $T^*_{rot} = 62$ K, the period is 9 ps.

excitation is the study by van Veen *et al.* with an excitation at 193 nm that populated the $v_2 = 2$ of the B 6s[2] state *via* 2^2_0 transition.[27] The reported anisotropy parameter of the methyl fragment was measured to be around $\beta = -0.36 \pm 0.05$ while that for the iodine was around $\beta = -0.72$, as expected for a shorter lifetime of 760 fs.[3]

This model suggests that ionization with a perpendicular probe polarization will show a different time dependence, as well as a less biased value of the predissociation time. The time-dependence for a perpendicular polarization of the 403 nm probe is shown in Fig. 9. Indeed, as expected, the measured CH_3 rise time is 1.359 ± 0.072 ps, as compared to 2.02 ± 0.15 ps when the probe polarization is parallel to that of the pump. As expected, the former value is similar to the measured decay time of the parent ion.

The bandwidths measured for the translational distributions of fragments $\nu_2 = 1$ (160 meV) and $\nu_2 = 2$ (121 meV) in Fig. 3c–d are significantly narrower than the translational distributions measured by Gitzinger *et al.*[7] This observation might be related to their slightly smaller value $\beta = -0.5$ for the anisotropy of the I* fragment. In particular, both observations are consistent with the conclusion that the expansion of the molecular beam (here a continuous beam and in Gitzinger's work a pulsed beam) can affect the time-scale of detection of the methyl and the observed angular distribution.

4.2 The iodine cation emitted parallel around 3 eV

The iodine distributions of Fig. 3 show that some fragments are produced with translational energies that exceed the available energy for dissociation to CH_3 + I* following excitation at 201.2 nm. For example, the fragments with translational energy of 3.50 eV observed in Fig. 3a exceed the available energy of 2.86 eV by approximately 22%. This unexpectedly high translational energy observed for the iodine fragment is not mirrored by the CH_3 co-fragment distribution. We can decompose our iodine distribution integrated over 360° in two components: one emitted perpendicular to the pump polarisation (~61%) and another one emitted parallel (~30%—see Fig. 3a). The perpendicular component is associated with the predissociation of the B 6s[2] state, and is consistent with the CH_3 energy distribution (see Fig. 5). The surprisingly high kinetic energy fragments are associated with the parallel component as shown in Fig. 7a. The time dependence of this parallel iodine is shown in Fig. 6c, as well as in Fig. 7b for different energies of the pump and probe. We will examine now the possible assignment of this contribution.

If this fast I signal resulted from dissociation into CH_3 + I, rather than I*, following excitation at 201.2 nm, the available energy would be sufficient to explain the observation. However, the observed kinetic energy of the I would indicate that it is produced in conjunction with CH_3 ($v_2 = 6, 7$), which would then be observed in the nonresonant CH_3 image (Fig. 3b). The absence of this CH_3 as well as the observation that the angular distribution of this I^+ is peaked along the pump polarisation (Fig. 7a) eliminates this potential explanation for the origin of the fast I signal.

One way to produce iodine ions without methyl cations is *via* the dissociation of CH_3I^+ into $CH_3(X^2A_2'') + I^+(^3P_2)$ with a (0 K) threshold 12.82 ± 0.02 eV above the CH_3I ground state.[31] The energetics of the cation are summarized in Fig. 1. Photoionization of CH_3I by 2 photons at 201.2 nm is known to leave the cation mostly in the $v = 0$ of the ground state $X^+E_{3/2}$ (at 9.538 eV).[6] Subsequent absorption of one probe photon will then increase the total excitation energy to 12.61 eV, just 355 meV above the threshold for dissociation to CH_3^+ + $I(^2P_{3/2})$. The first electronic excited state of CH_3I^+ is the $A(^2A_1)$ state whose minimum lies 2.4074 eV above the cation ground state. Transitions to the $A(^2A_1)$ state from the ground state are allowed with a transition dipole moment perpendicular to the C–I bond.[32] This $A(^2A_1)$ state correlates diabatically to the $CH_3(X^2A_2'') + I^+(^3P_2)$ asymptote. However, for low vibrational levels, fast internal conversion takes place back to the ground state, leading to the dissociation of the cation into CH_3^+ + I. Excitation by two extra probe photons will reach 15.7 eV ($2 + 2' - E_{kin}(e-)$). The second state of CH_3I^+ with $^2A_1$ symmetry lies around 15.22 eV, and is described as an excitation from the HOMO to the LUMO of the ion.[31] Another state occurs in this energy range, corresponding to the $B^2E_{3/2}$ state at about 15 eV, which is populated by a transition from a valence orbital into the partially filled HOMO.[31] The $B^2E_{3/2}$ state undergoes Jahn–Teller distortion, and the transition to the B state from the ground state of CH_3I^+ is broadened by internal conversion to the $A(^2A_1)$ state, followed by a dissociation into I^+ + CH_3.[33,34] The branching ratios measured in a PEPICO experiment (photoelectron-photoion coincidence) at 15.7 eV are 40% to CH_3 + I^+ and 60% to CH_2I^+ + H,[33] while the total energy released in the dissociation taking place at 15.8 eV is around 2.93 eV.[34] Photodissociation of CH_3I^+ by two photons has been already studied for wavelengths ranging from 427–720 nm.[32,35–38] These studies focused primarily on the low energy part of the A state by detecting the CH_3^+ fragment. Only Goss *et al.* have discussed the I^+ fragments appearance.[35] The two-photon transition $B(^2E_{3/2}) \leftarrow X(^2E_{3/2})$ can take place through a dipole transition either $A_1 \times A_1$ or $E \times E$. The first one will lead to I^+ emitted parallel to the probe polarisation while the second to I^+

emitted perpendicular to the probe polarisation which will thus be masked by the dominant contribution of the B 6s[2] state predissociation. Halogen atoms emitted parallel to the C–X axis following absorption into the B state have been already observed in the photodissociation of CH_3Br^+ and CH_3Cl^+ cations.[39,40] Note as well that in Fig. 4, the angular dependence of I^+ emitted parallel to the polarization axis is better fitted by assuming a two photon transition (blue line) than a one photon transition (black line): this fit supports our conclusion that the fast I^+ is produced by:

$$\begin{aligned} CH_3I &\xrightarrow{2\times\hbar\omega_{pump}} CH_3I^+(X^2E_{3/2}) + e^- \\ CH_3I^+(X^2E_{3/2}) &\xrightarrow{2\times\hbar\omega_{probe}} CH_3I^+(B^2E_{3/2}) \\ &\rightarrow CH_3(X^2A_2'') + I^+(^3P_2). \end{aligned} \quad (5)$$

Because the resonant step in the 1 + 1 ionization of CH_3I is a perpendicular transition, the C–I axis of the CH_3I^+ will initially be aligned perpendicular to the probe axis, and thus the two-photon parallel transition to the B state will not be efficiently excited until the rotation of the ion has brought the C–I axis parallel to the probe polarization. As in the case of the CH_3 detection discussed above, this rotation will take a while as observed in Fig. 6(c). The maximum translational energy expected for this channel is 2.9 eV, while the energy observed at long delay for iodine emitted parallel to the probe is 3 eV (see Fig. 7). This energy difference can be explained if some of the parent cations are produced with internal vibrational energy in the photoionization by two pump photons. This contribution is clearly visible in Fig. 7a for which the pump energy has been increased to enhance the production of cations by the pump alone, and the probe energy has been reduced to reduce the detection of the neutral iodine fragments produced by the predissociation from the neutral B state (around 2.8 eV).

5. Conclusion

We have investigated the predissociation of CH_3I from the vibrationless level of the B 6s[2] Rydberg state by imaging as a function of time the angular and translational energy distributions of the fragments. No I fragment has been detected leading us to conclude that the quantum yield of I* is close to 1. The dipole moment of this transition is perpendicular to the C–I axis leading to the ejection of iodine atoms mostly perpendicularly to the pump polarization. Instead, when the pump and probe polarizations are parallel to each other and to the detector plane, the CH_3 image angular distribution exhibits four-fold symmetry due a low detection sensitivity of the fragments flying perpendicularly to the pump laser polarization. This observation together with the fact that the angular distribution changes when changing the probe polarization indicates an alignment of CH_3 rotational angular momentum. Using resonant multiphoton ionization for the CH_3 fragments we could determine the vibrational energy distribution. The CH_3 products have excitation primarily in the umbrella mode as expected and observed in most of the dissociations of methyl halide. This distribution is peaked at $\nu_2 = 1$, with some minor activity in the ν_1 symmetric stretching as well. For this pump and probe polarization parallel configuration, while the iodine appears on a timescale in agreement with the decay time of the parent, the rise time of the main CH_3 fragment ($\nu_2 = 1$) is almost twice longer. We interpret this difference in the rising times of the two fragments as a result of a different sensitivity in the detection step. By considering the relative alignments of the transition dipoles used to photodissociate the CH_3I and to photoionize the CH_3 fragment with respect to the polarizations of the pump and the probe, we propose a model in which the rotation of the parent during predissociation alters the initial unfavorable alignment of the fragment C_3 axis to enable a delayed detection as observed experimentally. Both CH_3 angular distribution and the increased rising time are reflection of alignment effects and will be discussed in a forthcoming paper. By investigating their changes as a function of different relative configurations of the pump and probe polarizations, we will be able to shed more light onto this unexpected observations.

Two other contributions are observed in the I* kinetic energy distribution, corresponding to fragments emitted along the pump polarization. They appear on different timescales and are produced by multiphoton processes. One corresponds to the decay of 6p and 7s Rydberg states populated by a (1 + 1′) excitation and it was detected on the photoelectron spectrum as well.[6] Both I and I* seem to be produced by dissociation of one of these highly vibrationally excited Rydberg states. The present measurement gives an upper limit for the dissociation lifetime of one of these states, as being around 100 fs, namely the duration of the probe pulse. The second contribution comes from the dissociation by two probe photons of the CH_3I^+ produced with two photons of the pump onto $CH_3 + I^+$. As with the detection of the methyl fragment resonantly, this dissociation channel also depends on the rotational temperature of the parent molecule.

Note added in proof

González *et al*. have recently reported the observation of $I\ ^2P_{3/2}$ fragments following photodissociation of the $\nu_3 = 1$ band of the B state of CH_3I.[41]

Acknowledgements

This work was supported financially by the ANR COCOMOUV, the ANR HARMODYN and L'Université Paul Sabatier *via* three different BQR. S.T.P. thanks the CNRS for supporting invited research position in the LCAR. S.T.P. was also was supported by the U.S. Department of Energy, Office of Science, Office of Basic Energy Sciences, Division of Chemical Sciences, Geosciences, and Biosciences under contract No. DE-AC02-06CH11357. R.C. gratefully acknowledges the European Union for the award of an Intra-European Marie Curie fellowship through the contract MOLCOTUV-041732. D.S. acknowledges the European Union for its PhD fellowship from the ITN-ICONIC. We thank Elsa Baynard, Laurent Polizzi and Stéphane Faure for their expert technical assistance and Dr. Lionel Poisson for lending us his image analysis software.

References

1 J. C. Owrutsky and A. P. Baronavski, *Chem. Phys. Lett*., 1994, **222**, 335–338.
2 Z.-r. Wei, F. Zhang, Y.-m. Wang and B. Zhang, *Chin. J. Chem. Phys*., 2007, **20**, 419–424.
3 A. P. Baronavski and J. C. Owrutsky, *J. Chem. Phys*., 1998, **108**, 3445–3452.
4 A. H. Zewail and H. Guo, *Can. J. Chem*., 1994, **72**, 947–957.
5 D. Zhong, P. Y. Cheng and A. H. Zewail, *J. Chem. Phys*., 1996, **105**, 7864–7867.
6 N. Thire, R. Cireasa, V. Blanchet and S. T. Pratt, *Phys. Chem. Chem. Phys*., 2010, **12**, 15644–15652.
7 G. Gitzinger, M. E. Corrales, V. Loriot, G. A. Amaral, R. d. Nalda and L. Banares, *J. Chem. Phys*., 2010, **132**, 234313.
8 A. van den Brom, M. L. Lipciuc and M. H. M. Janssen, *Chem. Phys. Lett*., 2003, **368**, 324–330.
9 A. T. J. B. Eppink and D. H. Parker, *J. Chem. Phys*., 1999, **110**, 844.
10 R. d. Nalda, J. Dura, A. Garcia-Vela, J. G. Izquierdo, J. Gonzalez-Vazquez and L. Banares, *J. Chem. Phys*., 2008, **128**, 244309.
11 D. J. Donaldson, V. Veronica and N. Ron, *J. Chem. Phys*., 1987, **87**, 2522–2530.
12 G. C. G. Waschewsky, R. Horansky and V. Vaida, *J. Phys. Chem*., 1996, **100**, 11559–11565.
13 J. A. Syage and J. Steadman, *Int. J. Mass Spectrom. Ion Processes*, 1996, **159**, 125.
14 S. Eden, P. Limao-Vieira, S. V. Hoffmann and N. J. Mason, *Chem. Phys*., 2007, **331**, 232–244.
15 R. Ogorzalek Loo, H. P. Haerri, G. E. Hall and P. L. Houston, *J. Chem. Phys*., 1989, **90**, 4222–4236.
16 J. W. Hudgens, T. G. DiGiuseppe and M. C. Lin, *J. Chem. Phys*., 1983, **79**, 571.
17 H. B. Fu, Y. J. Hu and E. R. Bernstein, *J. Chem. Phys*., 2005, **123**, 234305–234307.
18 R. Locht, B. Leyh, H. W. Jochims and H. Baumgärtel, *Chem. Phys*., 2009, **365**, 109–128.
19 M. H. M. Janssen, D. H. Parker, G. O. Sitz, S. Stolte and D. W. Chandler, *J. Phys. Chem*., 1991, **95**, 8007–8013.
20 J. F. Black and I. Powis, *Chem. Phys*., 1988, **125**, 375–388.
21 F. Wang, M. L. Lipciuc, X. Yang and T. N. Kitsopoulos, *Phys. Chem. Chem. Phys*., 2009, **11**, 2234–2240.
22 A. T. J. B. Eppink and D. H. Parker, *J. Chem. Phys*., 1998, **109**, 4758–4767.
23 R. E. Continetti, B. A. Balko and Y. T. Lee, *J. Chem. Phys*., 1988, **89**, 3383–3384.
24 M. H. M. Janssen, M. Dantus, H. Guo and A. H. Zewail, *Chem. Phys. Lett*., 1993, **214**, 281–289.
25 A. B. Alekseyev, H.-P. Liebermann and R. J. Buenker, *J. Chem. Phys*., 2011, **134**, 044303–044308.
26 A. Gilchrist, G. Hancock, R. Peverall, G. Richmond, G. A. D. Ritchie and S. Taylor, *J. Phys. Chem. A*, 2008, **112**, 4531–4536.
27 G. N. A. van Veen, T. Baller and A. E. De Vries, *Chem. Phys*., 1985, **97**, 179–186.
28 B. A. Aleksey, L. Heinz-Peter, J. B. Robert and N. Y. Sergei, *J. Chem. Phys*., 2007, **126**, 234102.
29 C. Jonah, *J. Chem. Phys*., 1971, **55**, 1915–1922.
30 S.-c. Yang and R. Bersohn, *J. Chem. Phys*., 1974, **61**, 4400–4407.
31 R. Locht, *et al*., *J. Phys. B: At., Mol. Opt. Phys*., 2010, **43**, 105101.
32 M. Lee and M. S. Kim, *J. Chem. Phys*., 2007, **127**, 124313.
33 I. Powis, *Chem. Phys*., 1983, **74**, 421–432.
34 J. H. D. Eland, R. Frey, A. Kuestler, H. Schulte and B. Brehm, *Int. J. Mass Spectrom. Ion Processes*, 1976, **22**, 155–170.
35 S. P. Goss, D. C. McGilvery, J. D. Morrison and D. L. Smith, *J. Chem. Phys*., 1981, **75**, 1820–1828.
36 K. Walter, R. Weinkauf, U. Boesl and E. W. Schlag, *J. Chem. Phys*., 1988, **89**, 1914–1922.
37 A. M. Woodward, S. D. Colson, W. A. Chupka and M. G. White, *J. Phys. Chem*., 1986, **90**, 274–278.
38 Y. J. Bae and M. S. Kim, *J. Chem. Phys*., 2008, **128**, 124324.
39 V. Blanchet, P. C. Samartzis and A. M. Wodtke, *J. Chem. Phys*., 2009, **130**, 034304.
40 D. S. Won, M. S. Kim, J. C. Choe and T.-K. Ha, *J. Chem. Phys*., 2001, **115**, 5454–5460.
41 M. G. González, J. D. Rodríguez, L. Rubio-Lago and L. Bañares, *J. Chem. Phys*., 2011, **135**, 021102.

